Available online at www.sciencedirect.com
ScienceDirect
Journal of Power Sources 162 (2006) 1460–1466
JOURNAL OF POWER SOURCES
www.elsevier.com/locate/jpowsour

# The advanced carbide-derived carbon based supercapacitor

M. Arulepp [a,*], J. Leis [a,b], M. Lätt [a,b], F. Miller [a], K. Rumma [a,c], E. Lust [b], A.F. Burke [d]

[a] *Tartu Technologies Ltd., 185 Riia Str., 51014 Tartu, Estonia*
[b] *University of Tartu, 2 Jakobi Str., 51014 Tartu, Estonia*
[c] *Estonian Maritime Academy, 25 Mustakivi, 13912 Tallinn, Estonia*
[d] *University of California-Davis, 2003 Academic Surge, Davis, CA 95616, United States*

Received 19 May 2006; received in revised form 31 July 2006; accepted 3 August 2006
Available online 15 September 2006

**Abstract**

The electrical double-layer (EDL) performance of three different TiC-derived nanoporous carbon materials was tested in prismatic capacitor assembly filled with 1.2 M triethylmethylammonium tetrafluoroborate (TEMA) acetonitrile solution. The electrical double-layer characteristics of supercapacitors were studied using the cyclic voltammetry (CV) and the electrochemical impedance spectroscopy (EIS) methods. Energy density versus power density, i.e. Ragone plots were constructed from the constant resistance and constant power (CP) charge/discharge data. The 1450F supercapacitor with novel nanoporous carbon made by halogen treatment of TiC/$TiO_2$ composite demonstrated the energy density of more than 10 Wh $dm^{-3}$ at the cell voltage of 2.7 V.


*Keywords:* Carbide-derived carbon; Nonaqueous electrolyte; Electrical double-layer capacitor; Ragone plot

## 1. Introduction

The unique nanoporous structure of carbide-derived carbon (CDC) [1–2] together with the narrow pore size distribution and possibility to fine-tune the pore size as recently confirmed [3–6] has noticeably forced the development of applications requiring the nanoporous materials. More important applications proposed for CDC are fuel cells [7], different selective adsorption processes such as extraction/purification of noble gases [8], hydrogen storage [9], etc. However, one of the most challenging applications is the rapidly developing field of the electrochemical energy storing devices among them super- or ultracapacitors [10–12]. So far, the best CDC materials for supercapacitors have been made from titanium carbide (Eq. (1)) [13].

$$TiC + 2Cl_2 \rightarrow C + TiCl_4\uparrow \quad (1)$$

Although the carbon, derived from TiC below 900 °C, possesses BET surface area up to 1400 $m^2\,g^{-1}$ and is almost completely microporous [14], it has a serious disadvantage in practical use. These carbons contain a large quantity of very small nanopores with pore size below 6–7 Å, which are inaccessible to the solvated electrolyte ions [13,15]. To improve the penetrability of ions into the nanoporous carbon matrix, the oxidative post-treatment method has been used [16].

Recently a new method was developed, which enables to improve the pore size distribution in the carbide-derived carbon particles [17]. Using the chlorination of the carbide/oxide mixture, due to which the carbothermal reduction of $TiO_2$ in chlorine atmosphere gives the possibility to oxidise in situ the desired part of carbon during its formation from the carbide. The overall mass-balance of reagents and products of the chlorination process is given by the following equation (Eq. (2)):

$$TiC + xTiO_2 + 2(1+x)Cl_2 \rightarrow (1-x)C + (1+x)TiCl_4 + xCO_2 \quad (2)$$

where $x$ is a stoichiometrical constant corresponding to $TiO_2$ participating in reaction. In the chlorine atmosphere $TiO_2$ oxidizes the pre-determined small part of the carbon created during the etching of carbide with the chlorine and the process is well controlled by the amount of $TiO_2$ in the reaction medium. This method can be used for optimisation of the wettability and power characteristics of the supercapacitor electrodes using the nanoporous carbon powder discussed before.

* Corresponding author. Tel.: +372 7 383 057; fax: +372 7 428 467.
*E-mail address:* matia@park.tartu.ee (M. Arulepp).

0378-7753/$ – see front matter © 2006 Elsevier B.V. All rights reserved.
doi:10.1016/j.jpowsour.2006.08.014

Table 1
Pore structure characteristics of the carbon materials characterised in text, calculated from nitrogen and benzene sorption data

| | SkeletonC | $S_{BET}$ ($m^2\,g^{-1}$) | $S_L$ ($m^2\,g^{-1}$) | $V_P$ ($cm^3\,g^{-1}$) | $V_{MP}$ ($cm^3\,g^{-1}$) | $V_{P<11Å}$ ($cm^3\,g^{-1}$) | $V_{P>11Å}$ ($cm^3\,g^{-1}$) | $W_s$ ($cm^3\,g^{-1}$) |
|---|---|---|---|---|---|---|---|---|
| 1 | C(TiC) | 1348 | 1692 | 0.67 | 0.55 | 0.37 | 0.30 | 0.59 |
| 2 | C(TiC) + $H_2O$ | 1892 | 2454 | 1.03 | 0.67 | 0.11 | 0.92 | 0.94 |
| 3 | C(TiC/$TiO_2$) | 1588 | 2019 | 0.76 | 0.65 | 0.37 | 0.39 | 0.71 |

The main aim of the work described in this paper was to examine the performance of the $TiO_2$ assisted carbide-derived SkeletonC carbon in high-capacitance supercapacitors. Cyclic voltammetry (CV), constant current (CC), constant power (CP) and the electrochemical impedance spectroscopy (EIS) methods have been used. The results are compared with the previously prepared and tested TiC-derived carbon materials.

## 2. Experimental

### 2.1. The nanoporous carbon materials

Carbon powders were synthesised from titanium carbide (1–3 μm, H.C. Starck) using selective etching of TiC by chlorine at temperature 800–1000 °C [14]. The SkeletonC 1 was synthesised at 800 °C. SkeletonC 2 was synthesised at 970 °C, and additionally oxidised by water vapour at 900 °C. SkeletonC 3 was prepared by chlorinating the TiC/$TiO_2$ composite according to the method developed recently [17,18].

Porous structure of the carbon materials was characterised using different nitrogen and benzene sorption methods [19]. Low temperature nitrogen sorption experiments were performed using Gemini Sorptometer 2375 (Micromeritics). The specific surface area of the carbon materials was calculated according to BET and Langmuir theories ($S_{BET}$ and $S_L$, respectively), up to the nitrogen relative pressure ($P/P_0$) of 0.2. The total volume of pores, $V_P$, was calculated from nitrogen adsorption at relative pressure ($P/P_0$) of 0.95. The micropore volume, $V_{MP}$, was calculated from *t*-plot of the adsorption isotherm and the volumes of different pore size fractions, $V_{(P<11Å)}$ and $V_{(P>11Å)}$, were obtained from the data of BJH pore size distribution [19]. The size distribution of the micropores was calculated from the nitrogen sorption data measured by ASAP2000 (Micromeritics), using the method based on the density functional theory (DFT) [19].

Adsorption dynamics of benzene vapours at room temperature was studied using computer-controlled weighing method of the carbon samples in benzene vapours at normal pressure and room temperature in time.

Some selected sorption characteristics are presented in Table 1. The pore size distribution of the SkeletonC powders, calculated from the nitrogen sorption data by using the density functional theory, is compared in Fig. 1. The high-resolution HRTEM picture of SkeletonC 3 as recorded with the transmission electron microscope (JEOL JEM 3010 operated at 300 kV) is shown in Fig. 2.

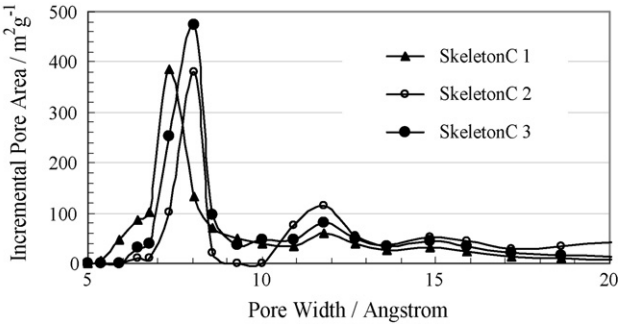


Fig. 1. Pore size distribution calculated using DFT method for different SkeletonC powders, derived from fine-grain TiC (H.C. Stack): without additives (triangles); for carbon with subsequent oxidation with water vapour (empty rings) and with 10%wt. $TiO_2$ additive in TiC at the beginning of chlorination (solid rings).

### 2.2. Preparation of the electrodes and capacitors

The polarizable carbon electrodes were prepared from the mixture of 92% (wt.) porous TiC-derived carbon powder and 8% (wt.) PTFE binder (Aldrich, 60% suspension in water) and rolled into the thin active material sheet with a final thickness of $90 \pm 5$ μm. After drying, the raw electrode sheets were plated from one side with a thin aluminium layer ($3 \pm 1$ μm) using the plasma activated-physical vapour-deposition method [12]. Former studies have strongly confirmed the importance of aluminium coating for reducing the contact resistance between carbon layer and current collector [20].

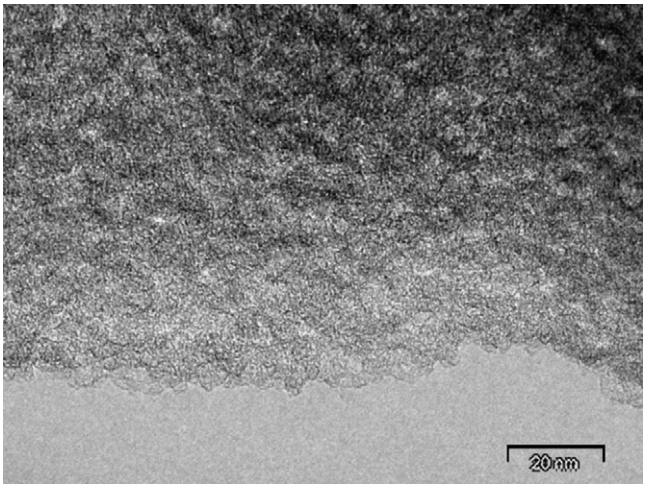


Fig. 2. HRTEM image of SkeletonC 3 prepared by chlorination the mixture of TiC and $TiO_2$, (10/1 weight ratio) at 800 °C.

The supercapacitor noted as SC 1450F was made from SkeletonC 3. The electrode package was assembled from wound pair of positive and negative electrodes, comprising aluminium coated carbon sheets connected to thin aluminium foil as current collectors, separated with an ion-permeable paper from Kodoshi Nippon (~30 μm thick). Six packages of positive and negative electrodes were connected in parallel and placed into the prismatic aluminium can (volume 136 $cm^3$). Total geometric surface area of electrode pairs was 3600 $cm^2$. The capacitor was dried prior impregnation with 1.2 M triethylmethylammonium tetrafluoroborate (TEMA, Stella) solution in anhydrous acetonitrile (AN, Riedel-de Haën, $H_2O < 0.003\%$). The TEMA salt was selected because of the use of highly nanoporous carbon materials in supercapacitors [18,21–23]. According to our preliminary studies $Et_3MeN^+$ cations yield higher specific electrical double-layer (EDL) capacitance compared to slightly bigger $Et_4N^+$ ions, commonly used in non-aqueous supercapacitors. Furthermore, the slightly weaker temperature dependence of electrical conductivity of TEMA/AN electrolyte compared to TEA/AN is expected to be preferable for achieving the high power densities in wide temperature range.

The comparative supercapacitor noted as SC 850F was made by using different nanoporous CDC electrodes. The positively charged electrodes, adsorbing anions, were made from SkeletonC 1; and the electrodes, adsorbing cations, were made from SkeletonC 2.

Before evaluation, the EDLC was kept at temperature +60 °C during 48 h. Thereafter, the continuous cycling from 2.7 to 1.35 V with the current $I = 6$ A was carried out prior performing the further electrochemical studies. The slight pressure created during preconditioning was released through the filling valve.

## 3. Results and discussion

### 3.1. Cyclic voltammetry and constant current studies

The cyclic voltammetry curves were recorded in the voltage range $\Delta U$ from 0 to 3 V using a potential sweep-rate $v$ from 0.5 to 2 mV $s^{-1}$ ($v = \pm dU/dt$). It was established that EDLCs are ideally polarizable in this voltage range applied. The cyclic voltammogram in Fig. 3 illustrates the capacitance versus voltage ($C$, $\Delta U$) relationship of prototype-supercapacitor in the voltage interval of 3 V.

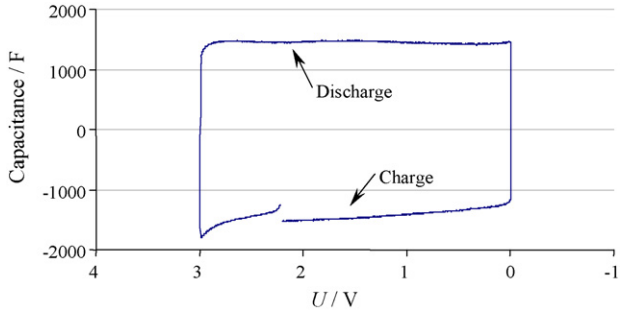


Fig. 3. Cyclic voltammogram expressed as capacitance vs. cell voltage for supercapacitor SC 1450F at scan rate 1 mV $s^{-1}$.

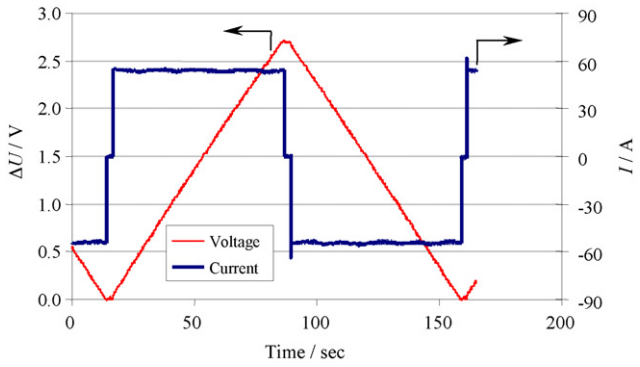


Fig. 4. Constant current charge/discharge profile of supercapacitor SC 1450F.

According to the data in Fig. 3, the capacitance of supercapacitor SC 1450F device slightly depends on the cell voltage applied. The increased capacitance at higher voltage has been caused mainly by the reduced effective size of the electrolyte ions adsorbed. This effect was recently observed and discussed for the SkeletonC carbon electrodes [21–23]. It should be noted that, the capacitance increases exponentially with charging the capacitor over $\Delta U = 2.8$ V, indicating the occurrence of faradaic processes. For this reason the voltage below 2.7 V has been typically used for the nonaqueous EDLCs.

Additionally the EDLC capacitor was studied at constant current charge/discharge regimes in the voltage range from 0 to 2.7 V. The current was varied from 6 to 315 A, respectively. The discharge capacitance was calculated from the data of the third cycle according to the Eq. (4).

$$\bar{C} = I\frac{\Delta t}{\Delta U} \tag{4}$$

The internal resistance values were calculated from the value of initial potential drop, (so-called IR-drop) at fixed $dt = 10$ ms according to the Eq. (5).

$$R = \frac{dU_1}{I} \tag{5}$$

The constant current charge-discharge cycling data in Fig. 4 are given for illustrating the dependence of capacitance and resistance on the current applied.

The capacitance of the supercapacitor SC 1450F was calculated at different current values used, and the total capacitance of the cell depends weakly on the current applied. Although, there are many different techniques for the evaluation of the nominal capacitance, it is generally accepted that the reasonable current value applied in the testing should be ~5 mA $farad^{-1}$ [24]. However, in present study the higher current values were also applied to explore the applicability limits of the capacitor.

Charge/discharge profiles in Fig. 5 are particularly characterised with the IR-drop, well seen before and after small constant voltage plateau, which originates from the internal resistance of the capacitor.

The voltage/time curves at constant current charge/discharge regime have nearly linear shape for all current ranges studied. The calculated gravimetric capacitance at $I = 6$ A, presented in Table 2, is rather similar for different TiC-derived SkeletonC

Table 2
Capacitance characteristics of Supercapacitors tested at room temperature

| Carbon origin | Capacitance (F) | Density of electrode (g cm$^{-3}$) | Specific capacitance of | | | |
|---|---|---|---|---|---|---|
| | | | Device[a] | | Carbon[b] | |
| | | | (F cm$^{-3}$) | (F g$^{-1}$) | (F cm$^{-3}$) | (F g$^{-1}$) |
| TiC/TiO$_2$ | 1450 | 0.71 | 10.7 | 7.3 | 87 | 122 |
| TiC | 869 | 0.55 | 6.4 | 5.0 | 66 | 120 |

[a] Calculated per weight and volume of completed device, wt. 200 g, vol. 136 cm$^3$.
[b] Calculated per dry weight and volume of single electrodes, CC regime.

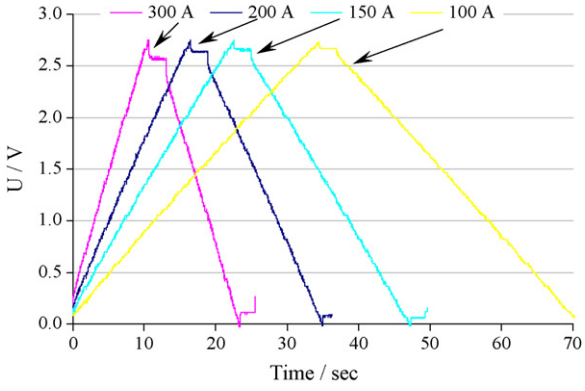


Fig. 5. Constant current charge/discharge profile of supercapacitor SC 1450F at different current values.

materials [18]. It should be noted that the capacitance of nanoporous carbide-derived carbon decreases monotonically with increasing the charging current [21].

The data obtained using constant current charge/discharge regime are presented in Table 3. According to the results established, the delivered charge and capacitance decrease with increasing the current applied. The achieved energy ($E_{out}$) depends on the value of cycling current. The ratio of achieved energy ($E_{out}$) and applied energy ($E_{in}$) yields the round-trip efficiency (RTE).

The so-called joule-based RTE values for the EDLC assume that the current of 315 A corresponds to the current density of 2.1 A cm$^{-3}$ and power density of 2.8 kW L$^{-1}$. It has to be mentioned that the so-called coulomb-based round trip efficiency of supercapacitor SC 1450F reach nearly 100% under study of this work.

### 3.2. Constant power studies

Constant power discharge tests of the supercapacitor SC 1450F were performed at the University of California-Davis, Davis, CA, United States. Power levels were chosen so that the discharge times varied from about 60 s to less than 10 s. The corresponding power density levels varied from 250 to 2500 W kg$^{-1}$. The results of the tests are given in Table 4. Note that the energy density was ~5.2 Wh kg$^{-1}$ for the complete range of the power densities tested, which indicates that the supercapacitor under study is a very high power device. This

Table 3
Constant current charge-discharge data for supercapacitor SC 1450F

| $I$ (A) | $R$ (mΩ) | $Q$ (As) | $C$ (F) | Duration (s) | $E_{in}$ (J) | $E_{out}$ (J) | RTE (%) |
|---|---|---|---|---|---|---|---|
| 6 | – | 3915 | 1450 | 649 | 5371 | 5285 | 98.4 |
| 10 | – | 3904 | 1446 | 389 | 5362 | 5271 | 98.3 |
| 55 | 0.33 | 3792 | 1420 | 69.6 | 5365 | 5082 | 94.7 |
| 107 | 0.33 | 3670 | 1417 | 34.2 | 5391 | 4802 | 89.1 |
| 158 | 0.33 | 3533 | 1386 | 22.3 | 5460 | 4547 | 83.3 |
| 213 | 0.32 | 3468 | 1360 | 16.3 | 5326 | 4375 | 82.1 |
| 267 | 0.32 | 3382 | 1353 | 12.7 | 5544 | 4181 | 75.4 |
| 315 | 0.32 | 3287 | 1336 | 10.4 | 5295 | 3940 | 74.4 |

Table 4
Constant power discharge data and round-trip efficiency for the supercapacitor SC 1450F

| Power (W) | Time (s) | Discharge[a] | | | | | Charge (W s) | Round-trip efficiency |
|---|---|---|---|---|---|---|---|---|
| | | (W s) | (Wh kg$^{-1}$) | (W kg$^{-1}$) | (Wh L$^{-1}$) | (W L$^{-1}$) | | |
| 50 | 73.6 | 3680 | 5.10 | 250 | 7.5 | 367 | 3836 | 0.959 |
| 130 | 29 | 3770 | 5.24 | 650 | 7.7 | 955 | 3816 | 0.988 |
| 250 | 14.7 | 3675 | 5.10 | 1250 | 7.5 | 1838 | 3804 | 0.966 |
| 400 | 9.6 | 3840 | 5.33 | 2000 | 7.8 | 2941 | 3935 | 0.976 |
| 500 | 7.4 | 3700 | 5.14 | 2500 | 7.5 | 3676 | 3909 | 0.946 |

[a] Discharge from 2.7 to 1.35 V, charge at 100 A, held at 2.7 V for 60 s; weight and volume of SC 1450F were 200 g and 136 cm$^3$.

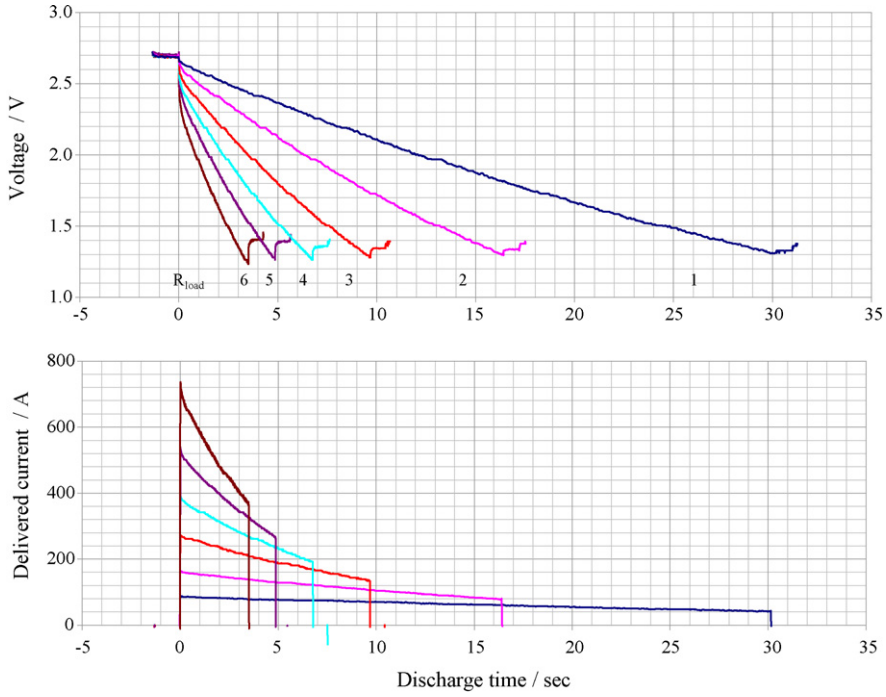


Fig. 6. Discharge curves for the supercapacitor SC 1450F by using different constant resistance $R_{load}$ values applied.

is not surprising in that the RC time constant of this device is 0.47 s. The pulse power capability of a supercapacitor can be expressed as $P = 9/16\ (1-EF)U^2/R$, where $EF$ is the discharge efficiency. The calculated pulse power of SC 1450F for a 95% efficiency is high, 3110 W kg$^{-1}$. Also as indicated in Table 4, the round-trip efficiencies for a complete charge and discharge of the device are 95% and somewhat higher for constant power density ranging up to 2500 W kg$^{-1}$.

The volumetric energy density of the device is ~7.6 Wh L$^{-1}$ for the complete range of the tests. According to the data in Table 4 the performance of the SC 1450F is excellent in terms of both energy storage and power capability.

### 3.3. Discharge of capacitors at constant resistance regime

To evaluate the performance and output power of large capacitors the constant resistance discharge (CRD) testing mode has been used. The essence of this method is that the resistance of the load into which electrical power is delivered remains constant throughout discharge cycle. The capacitor was charged to 2.7 V with constant current ~60 A and thereafter discharged throughout the load resistance ($R_{load}$). A small pause (1 s) was used between each charge/discharge cycle due to the technical reasons. $R_{load}$ was varied from 30 to 0.9 mΩ, whereby the data of the third cycle were recorded for each $R_{load}$ applied.

This technique allows achieving rather high power values, depending on the internal resistance $R_{internal}$ of the capacitor tested. The parameters recorded are presented in Fig. 6 and Table 5. It is important to mention that CRD method requires the integration of many parameters ($Q$, $P_{average}$, $E$), because $I$, $E$ and $P$ are not constant in time.

The data obtained from constant power charge/discharge cycles in Table 4 and from the constant resistance discharge data in Table 6 were used for constructing the Ragone plots presented in Fig. 7. A good agreement between the results obtained using two discharge methods confirms a reliability of both evaluation methods used for testing the supercapacitor SC 1450F.

### 3.4. Electrochemical impedance study

Electrochemical impedance spectroscopy analysis is based on the Nyquist $Z''$,$Z'$-plot method, where $Z''$ and $Z'$ are the imaginary and real parts of the complex impedance. Mathematically,

Table 5
Constant resistance discharge data for the supercapacitor SC 1450F

| $R_{load}$ (#) | $R_{load}$ (mΩ) | $I_{max}$ (A) | $I_{min}$ (A) | $I_{average}$ (A) | $\Delta t$ (s) | $Q$ (A s) | $E$ (J) | $P_{max}$ (W) | $P_{min}$ (W) | $P_{average}$ (W) |
|---|---|---|---|---|---|---|---|---|---|---|
| 1 | 27.16 | 88 | 42 | 63 | 28.86 | 1829 | 3667 | 234 | 58 | 127 |
| 2 | 13.72 | 162 | 83 | 118 | 15.54 | 1828 | 3635 | 437 | 111 | 234 |
| 3 | 6.9 | 272 | 139 | 200 | 9.00 | 1801 | 3525 | 714 | 188 | 392 |
| 4 | 4.1 | 389 | 203 | 285 | 6.13 | 1751 | 3381 | 1009 | 272 | 551 |
| 5 | 2.1 | 539 | 288 | 392 | 4.40 | 1723 | 3277 | 1370 | 387 | 745 |
| 6 | 0.9 | 736 | 405 | 539 | 3.01 | 1621 | 3000 | 1813 | 545 | 998 |

Table 6
Different specific characteristics of the supercapacitor SC 1450F, derived from the data in Table 5

| $R_{load}$ (#) | $E$ (Wh kg$^{-1}$) | $E$ (Wh L$^{-1}$) | $P$ (KW L$^{-1}$) | $P$ (KW kg$^{-1}$) | $R_{internal}$ (mΩ) |
|---|---|---|---|---|---|
| 1 | 5.09 | 7.49 | 0.93 | 0.64 | 0.32 |
| 2 | 5.05 | 7.42 | 1.72 | 1.17 | 0.27 |
| 3 | 4.89 | 7.20 | 2.88 | 1.96 | 0.27 |
| 4 | 4.69 | 6.91 | 4.05 | 2.76 | 0.30 |
| 5 | 4.55 | 6.69 | 5.48 | 3.72 | 0.33 |
| 6 | 4.17 | 6.13 | 7.34 | 4.99 | 0.32 |

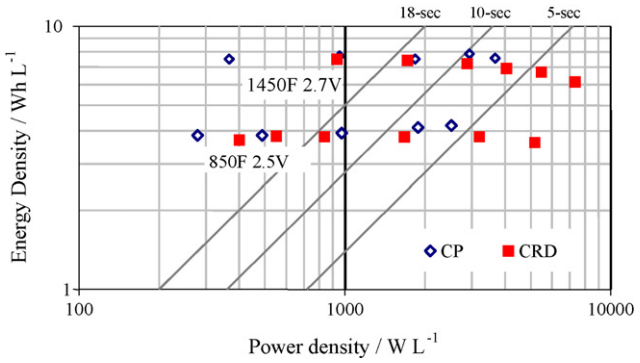


Fig. 7. Ragone plot for supercapacitors SC 1450F and SC 850F evaluated by constant power (CP) and constant resistance discharge (CRD) methods (discharging of EDLC to 1/2 of working voltage $\Delta U$).

$Z'$ and $Z''$ are connected according to the equation

$$Z = Z' + Z'' = R + \frac{1}{j\omega C} \quad (6)$$

from which $R$ and $C$ can be determined by using well-known frequency-response analysis method [10].

$Z''$,$Z'$-plots, presented in Fig. 8a confirm that the EDLC behaves as a typical capacitor over the frequency range from 100 Hz to 10 mHz. The EIS data for supercapacitor SC 1450F show that the knee point in the $Z''$,$Z'$-plot (Fig. 8a) has a frequency 0.5 Hz. Below ac frequency 0.5 Hz the maximum adsorption of the ions into the nanopores takes place and the capacitance is almost independent of the ac frequency applied. At $Z'' = 0$, $Z'$ demonstrates the lowest resistance value of the capacitor tested.

The length and characteristics of the plateau in the $Z''$,$Z'$-plots with the ∼45° slope (so-called diffusion limited porous region in Fig. 8a) depend on many factors, including temperature, electrode thickness and carbon, separator and electrolyte characteristics, etc. In the high ac frequency region, the porous electrode behaves like a planar surface and therefore, the capacitance obtained is by many orders of magnitude lower compared to the equilibrium capacitance obtained at $\omega \to 0$. This region of $Z''$,$Z'$-plots (usually at $f = 10$ Hz or 100 Hz) is used to determine the internal resistance of the double-layer capacitor, $Z'_{(\omega \to 0)} = R_{int}$. The capacitors with very high capacitance and very low impedance values have limiting $Z'_{(\omega \to 0)}$ values at frequencies below 100 Hz. Therefore, usually ac frequency equal to 10 Hz are used for obtaining the value of $R_{int}$ for the capacitors.

Fig. 8b shows the phase angle versus ac frequency relationship for EDLC. Theoretically, the capacitor behaves ideally when $\delta \approx -90°$, and the experimental fact that the cells containing more nanoporous carbon having only slightly lower absolute phase angle values than −90° indicates that this deviation may be caused by the specific interactions between the solvent and nanoporous carbon surface [8].

Fig. 9(a–b) shows the series capacitance $C_S$ and series resistance $R_S$ dependencies on the ac frequency applied to supercapacitor. According to the EIS data the capacitance value reaches almost 1450F at 10 mHz, whereby the resistance is only 0.31 mΩ at 10 Hz. Thus, the EIS capacitance is almost equal to the value observed using CC measurement method at current density 5 mA cm$^{-2}$. However, the resistance values obtained with using these two methods are somewhat different due to the technical regimes used for the testing. The similar discrepancies between

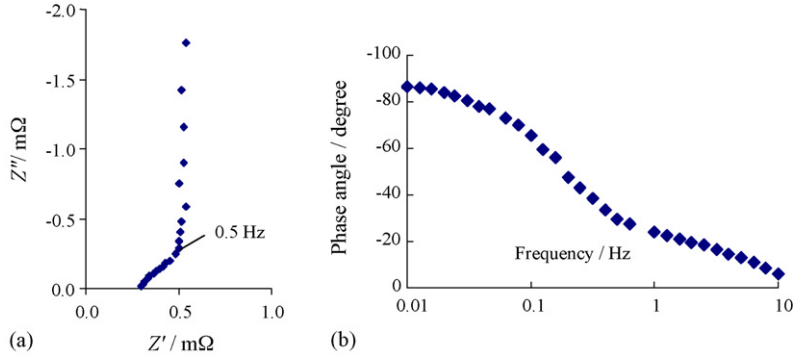


Fig. 8. Nyquist (a) and phase angle vs. frequency plot (b) for the supercapacitor SC 1450F.

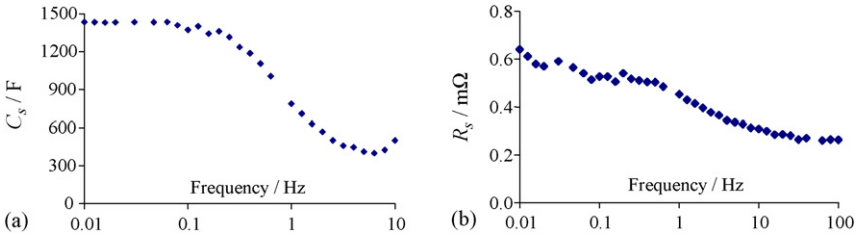


Fig. 9. Series capacitance $C_S$ (a) and series resistance $R_S$ (b) vs. frequency plots for supercapacitor SC 1450F.

the resistance values obtained using EIS and CC methods were observed in many papers [21–23].

## 4. Conclusions

The novel nanoporous carbide-derived carbon having improved pore size distribution was synthesised by chlorinating the TiC/$TiO_2$ composite. The BET surface area of carbon synthesised was 1590 $m^2\,g^{-1}$. The EDL-capacitor device was built up with the total volume of 136 $cm^3$. Electrochemical and electrical double-layer characteristics of the novel carbon material in the 1.2 M solution of triethylmethylammonium tetrafluoroborate in acetonitrile was studied, using the cyclic voltammetry and the electrochemical impedance spectroscopy methods.

It was shown that the carbide-derived carbon material used in our supercapacitor SC 1450F demonstrates excellent EDLC characteristics. Although the specific gravimetric capacitance of the novel carbon (120 $F\,g^{-1}$) does not surpass the advanced activated carbon materials, however, the volumetric capacitance over 90 $F\,cm^{-3}$ is highest, so far established for nonaqueous EDL capacitors. Evidence of quick faradaic reactions was not observed using the working voltage up to 2.7 V. The internal resistance of supercapacitor SC 1450F was 0.31 mΩ, and the stored energy density 10.8 $Wh\,L^{-1}$ at cell voltage 2.7 V has been calculated.

The constant power and constant resistance discharge data were compared, using the Ragone plot method. A very good agreement between the results confirms a reliability of both evaluation methods used in this work.

## Acknowledgements

The authors wish to thank colleagues from Tartu Tehnoloogiad for the kind assistance in preparing Supercapacitors, and UC Davis performing the comparative experiments. Dr. Gunnar Svensson, Stockholm University, is thanked for the HRTEM study of carbon materials.

## References

[1] G. Yushin, A. Nikitin, Y. Gogotsi, in: Y. Gogotsi (Ed.), Nanomaterials Handbook, CRC press, Taylor & Francis Group, USA, 2006, pp. 239–282.
[2] A. Nikitin, Y. Gogotsi, in: H.S. Nalwa (Ed.), Encyclopedia of Nanoscience and Nanotechnology, 7, American Scientific Publishers, Stevenson Ranch, CA, USA, 2003, pp. 553–574.
[3] R.N. Kyutt, E.A. Smorgonskaya, A.M. Danishevski, S.K. Gordeev, A.V. Grechinskaya, Phys. Solid State 41 (1999) 1359–1363.
[4] J. Leis, A. Perkson, M. Arulepp, M. Käärik, G. Svensson, Carbon 39 (2001) 2043–2048.
[5] A. Perkson, J. Leis, M. Arulepp, M. Käärik, S. Urbonaite, G. Svensson, Carbon 41 (2002) 1729–1735.
[6] Y. Gogotsi, A. Nikitin, H. Ye, W. Zhou, J.E. Fischer, B. Yi, H.C. Foley, M.W. Barsoum, Nat. Mater. 2 (2003) 591–594.
[7] A. Jerome. Mixed reactant molecular screen fuel cell, US 2005/0058875 (2005).
[8] H. Simgen, G. Heusser, G. Zuzel, Appl. Radiat.Isot. 61 (2004) 213–217.
[9] E. Johansson, B. Hjörvarsson, T. Ekström, M. Jacob, J. Alloys Compd. 330–332 (2002) 670–675.
[10] B.E. Conway, Electrochemical Supercapacitors. Scientific Fundamentals and Technological Applications, Kluwer Academic Publishers, Plenum Press, New York, 1999.
[11] A.W. Burke, J. Power Sources 91 (2000) 37–50.
[12] Y. Maletin, et al., Supercapacitor and a method of manufacturing such a supercapacitor, WO 02/39468 (2002).
[13] M. Arulepp, Electrochemical characteristics of porous carbon materials and electrical double layer capacitors. Dissertationes Chimicae Universitatis Tartuensis, vol. 38, Tartu University Press, (2003).
[14] J. Leis, A. Perkson, M. Arulepp, P. Nigu, G. Svensson, Carbon 40 (2002) 1559–1564.
[15] O. Barbieri, M. Hahn, A. Herzog, R. Kötz, Carbon 43 (2005) 1303–1310.
[16] J. Leis, M. Arulepp, A. Perkson. Method to modify pore characteristics of porous carbon and porous carbon materials produced by the method, WO 2004/094307 (2004).
[17] J. Leis, M. Arulepp, M. Lätt, H. Kuura. A method of making the porous carbon material and porous carbon materials produced by the method, PCT/EE2005/000007 (2005).
[18] J. Leis, M. Arulepp, A. Kuura, M. Lätt, E. Lust, Carbon 44 (2006) 2122–2129.
[19] S.J. Gregg, K.S.W. Sing, Adsorption, Surface Area and Porosity, Academic Press, London, 1982.
[20] Y. Maletin, E. Shembel, P. Novak, N. Stryzhakova, et al., Proceedings of the 15th International Seminar on Double Layer Capacitors And Hybrid Energy Storage Devices, Deerfield Beach, USA, 2005, pp. 125–129.
[21] M. Arulepp, L. Permann, J. Leis, A. Perkson, K. Rumma, A. Jänes, E. Lust, J. Power Sources 133 (2004) 320–328.
[22] E. Lust, G. Nurk, A. Jänes, M. Arulepp, L. Permann, P. Nigu, P. Möller, Condens. Matter Phys. 5 (2002) 307.
[23] L. Permann, M. Lätt, J. Leis, M. Arulepp, Electrochim. Acta 51 (2006) 1274–1281.
[24] P. Kurzweil, B. Frenzel, R. Gallay, Proceedings of the 15th International Seminar on Double Layer Capacitors And Hybrid Energy Storage Devices, Deerfield Beach, USA, 2005, pp. 14–25.